Pre-Steady-State Analysis of the Nucleoside Hydrolase of *Trypanosoma vivax*. Evidence for Half-of-the-Sites Reactivity and Rate-Limiting Product Release[†]

An Vandemeulebroucke,* Wim Versées, Stefan De Vos, Els Van Holsbeke, and Jan Steyaert

Department of Ultrastructure, Vlaams Interuniversitair Instituut voor Biotechnologie, Vrije Universiteit Brussel, Pleinlaan 2, 1050 Brussel, Belgium

Received May 14, 2003; Revised Manuscript Received August 8, 2003

ABSTRACT: The nucleoside hydrolase (NH) of the *Trypanosoma vivax* parasite catalyzes the hydrolysis of the *N*-glycosidic bond in ribonucleosides according to the following reaction: β-purine (or pyrimidine) nucleoside + H_2O → purine (pyrimidine) base + ribose. The reaction follows a highly dissociative nucleophilic displacement reaction mechanism with a ribosyl oxocarbenium-like transition state. This paper describes the first pre-steady-state analysis of the conversion of a number of purine nucleosides. The NH exhibits burst kinetics and behaves with half-of-the-sites reactivity. The analysis suggests that the NH of *T. vivax* follows a complex multistep mechanism in which a common slow step different from the chemical hydrolysis is rate limiting. Stopped-flow fluorescence binding experiments with ribose indicate that a tightly bound enzyme−ribose complex accumulates during the enzymatic hydrolysis of the common purine nucleosides. This is caused by a slow isomerization between a tight and a loose enzyme−ribose complex forming the rate-limiting step on the reaction coordinate.

The nucleoside hydrolases (NHs,[1] EC 3.2.2.1) catalyze the hydrolysis of the *N*-glycosidic bond in ribonucleosides according to the following reaction: β-purine (or pyrimidine) nucleoside + H_2O → purine (pyrimidine) base + ribose. The NHs are members of a larger functional family of *N*-ribohydrolases and transferases including the purine-nucleoside phosphorylases (*1*) and the phosphoribosyl transferases (*2*, *3*) and play a key role in the purine salvage pathway of protozoan parasites.

On the basis of their substrate specificity, the NHs are divided into three subclasses: the base aspecific inosine−uridine preferring nucleoside hydrolases (IU-NH) (*4*), the purine specific inosine−adenosine−guanosine preferring nucleoside hydrolases (IAG-NH) (*5*, *6*), and the 6-oxo-purine specific inosine−guanosine preferring nucleoside hydrolases (IG-NH) (*7*). The nucleoside hydrolase from *Crithidia fasciculata* is the best-known representative of the IU-NH subclass. The enzyme follows a highly dissociative nucleophilic displacement reaction mechanism with a ribosyl oxocarbenium-like transition state (*8*, *9*). The expulsion of the base is facilitated by protonation of the N-7 of the purine ring before reaching the transition state. The nucleoside hydrolase from *Trypanosoma vivax* (*T. vivax*) is the best-characterized IAG-NH. Both enzymes, IU-NH as well as IAG-NH, share a similar ribose binding site: all residues interacting with the ribose and a catalytic Ca^{2+} ion are conserved in the amino acid sequences and superimpose very well in the structure. The different substrate specificity between IU-NHs and IAG-NHs is reflected by a much greater divergence in the protein structure around the base of a bound substrate (*5*).

Previously, we investigated the enzyme−substrate interactions of the *T. vivax* IAG-NH using steady-state kinetic measurements and protein engineering techniques (*10*). The *T. vivax* IAG-NH hydrolyzes inosine, adenosine, and guanosine most efficiently. These reactions are catalyzed at very similar rates, and the k_{cat} values for these substrates are rather low ($\approx$4 s^{-1} at pH 7.0). In total, 12 amino acids within interaction distance to the substrate were replaced by alanine (*10*). Strikingly, only very few mutations caused a considerable effect on the steady-state turnover number (k_{cat}). Here, we perform the first pre-steady-state analysis on the *T. vivax* IAG-NH. This analysis suggests that the *T. vivax* enzyme follows a complex multistep mechanism in which a common slow step, different from the chemical hydrolysis, is rate limiting.

MATERIALS AND METHODS

Expression and Purification of the T. vivax IAG-NH. Expression and purification of the wild type and Asp10Ala mutant of the *T. vivax* IAG-NH were performed as described previously (*5*). The *Escherichia coli* strain WK6 containing the *T. vivax iagnh* open reading frame cloned in the pQE-30 expression vector was used to express the protein. The presence of an N-terminal His_6-tag allowed for a two-step purification scheme, consisting of a Ni-NTA affinity chromatography step (Qiagen) and gel filtration on a superdex-200 column (Amersham Bioscience). SDS−polyacrylamide gel electrophoresis was used to confirm enzyme purity. The

[†] This work was supported in part by the Vlaams Interuniversitair Instituut voor Biotechnologie and the Nationaal Fonds voor Wetenschappelijk Onderzoek-Vlaanderen. W.V. was supported by a grant from the FWO-Vlaanderen.

* Corresponding author. Tel: +32-2-6291851. Fax: +32-2-6291963. E-mail: avdemeul@vub.ac.be.

[1] Abbreviations: NH, nucleoside hydrolase; Ni-NTA, nickel-nitrilotriacetic acid; HEPES, [4-(2-hydroxyethyl)-1-piperazineethanesulfonic acid]; E, enzyme; ES, enzyme−substrate complex; B, base; ER, enzyme−ribose complex; R, ribose.

10.1021/bi0347914 CCC: $25.00
Published on Web 10/16/2003

concentration of pure protein (expressed per subunit) was determined spectrophotometrically using a ϵ_{280} of 47 752 M^{-1} cm^{-1} (*11*). Typically, 80 mg of purified protein was obtained from a 1 L fermentation.

Stopped-Flow Experiments. Stopped-flow experiments were performed on an Applied Photophysics model SX18.MV stopped-flow spectrofluorimeter fitted with a Xenon lamp. All experiments were performed at 35 °C in a 20 mM HEPES buffer pH 8.0. Volumes of 200 μL were injected from each syringe, and the reported concentrations are those in the reaction chamber.

Stopped-Flow Absorption Experiments. Stopped-flow absorption was used to follow the enzymatic release of the bases guanine, hypoxanthine, or adenine from guanosine, inosine, and adenosine in the steady state and pre-steady state. The difference in absorption between the nucleoside and the produced base causes a decrease in absorption upon hydrolysis. The $\Delta\epsilon$ values (mM^{-1} cm^{-1}) used were: guanosine, −4 at 253 nm, inosine, −1.3 at 250 nm, and adenosine, −0.9 at 250 nm. A path length of 1 cm was used throughout the stopped-flow absorption experiments.

For the pre-steady-state experiments, the substrate was used in excess (>5-fold) to the enzyme, allowing the assumption that the association of the substrate is very fast as compared to the subsequent steps during the first turnover. Experimental data were first transformed in traces of product concentration in a function of time using software supplied with the stopped-flow apparatus. The amplitude of the burst (π) and the initial rate of the steady-state phase (k_{ss}) were determined using a linear regression on the steady-state part of the progress curve (between 0.1 and 0.2 s) according to the following equation (*12*):

$$[\text{base}] = k_{ss}e_0t + \pi \quad (1)$$

In a next step, the traces were fitted to the standard equation for burst kinetics (*12*) using the program Origin (Microcal):

$$[\text{base}] = \frac{k_2k_3e_0t}{k_2 + k_3} + \frac{k_2^2e_0\{1 - \exp[-(k_2 + k_3)t]\}}{(k_2 + k_3)^2} \quad (2)$$

For long times, this equation corresponds to a linear behavior $[\text{base}] = k_{ss}e_0t + \pi$, with $\pi = k_2^2/(k_2 + k_2)^2$ and $k_{ss} = k_2k_3/(k_2 + k_3)$. To determine the steady-state catalytic parameters for guanosine, stopped-flow absorption measurements were performed at lower enzyme concentrations and over larger time intervals. The data were fitted to the Michaelis−Menten equation using the program Origin (Microcal).

Stopped-Flow Fluorescence Quenching Experiments. The binding of ligands into the active site of the *T. vivax* IAG-NH quenches the tryptophan fluorescence of the protein significantly. On the basis of this phenomenon, we used stopped-flow fluorescence to study the kinetics of ribose, substrate (guanosine), or inhibitor (3-deaza adenosine) binding to the enzyme. We also used stopped-flow fluorescence to follow the formation of ligand-bound enzyme intermediates during substrate conversion in multiple turnover experiments. Upon excitation at 280 nm, tryptophan fluorescence changes were followed above 310 nm using a 310 nm cutoff filter. The kinetic traces of ligand binding were analyzed by a nonlinear regression routine implemented in the stopped-flow software. All traces could be fitted with either a single or a double exponential. The observed relaxation rates were analyzed over the examined ligand concentration range. In the case of a two-step association mechanism, the general solution for the relaxation rates k_{obs1} and k_{obs2} (*19*) are given by

$$k_{obs_1} = \frac{1}{2}\{\sum k + \sqrt{(\sum k)^2 - 4\Pi k}\} \text{ and}$$

$$k_{obs_2} = \frac{1}{2}\{\sum k - \sqrt{(\sum k)^2 - 4\Pi k}\} \quad (3)$$

with

$$\sum k = k_1[\text{L}] + k_{-1} + k_2 + k_{-2} \text{ and}$$

$$\Pi k = k_1[\text{L}]k_2 + k_1[\text{L}]k_{-2} + k_{-1}k_{-2}$$

Where k_{obs1} and k_{obs2} are the relaxation rates derived from the kinetic traces, and [L] is the ligand concentration.

When both relaxations are on a different time scale (in this case, $k_{obs1} \gg k_{obs2}$), they can be dealt with separately, and the following equations can be used to derive the microscopic rate constants (*14*):

$$k_{obs_1} = k_{-1} + k_1[\text{L}] \text{ and } k_{obs_2} = k_{-2} + k_2\frac{[\text{L}]}{[\text{L}] + K_s} \quad (4)$$

The overall dissociation constant K_{SO} for this two-step association mechanism was derived from the following equation (*19*):

$$K_{SO} = \frac{K_s}{1 + (k_2/k_{-2})} \quad (5)$$

where K_S is the dissociation constant for the first bimolecular step.

Fitting with Pro-Kinetics II (Pro-KII). Pro-KII (Applied Photophysics Ltd.) is a software package that allows a simultaneous analysis of a series of kinetic traces according to a proposed reaction scheme and provides a best-fit parameter set accommodating all kinetic behavior across the entire concentration range.

RESULTS

Burst Kinetics of Guanosine Hydrolysis. To detect transient intermediates, we examined the pre-steady-state release of guanine upon hydrolysis of guanosine using stopped-flow absorption. Guanosine was chosen as the model substrate because its hydrolysis causes large changes in absorption. Upon mixing the enzyme (3−10 μM) with an excess of guanosine (50 μM), the formation of guanine follows characteristic burst kinetics (Figure 1) indicative for at least two transient intermediates.

The amplitude of the burst (eq 1), observed during the first turnover, shows that only one nucleoside base is released per two active sites. To confirm this observation, an active site titration was conducted with the substrate guanosine. The maximum amplitude of the burst of product formation per enzyme subunit (π/[e]) is 0.52 mol/mol ± 0.04. Comparable values were obtained using different batches of purified enzyme. Considering that the *T. vivax* enzyme appears as a homodimer in solution, these results indicate that this enzyme exhibits half-of-the-sites reactivity.

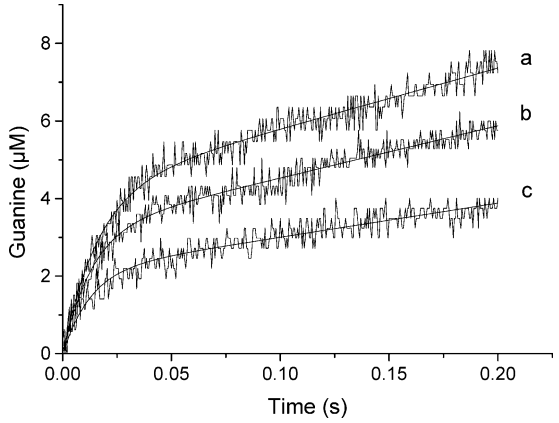

FIGURE 1: Burst kinetics of guanosine hydrolysis. Bursts of guanine formation observed upon mixing a different concentration of *T. vivax* NH (a, 9.94 μM; b, 7.45 μM; and c, 4.96 μM) with an excess of guanosine (50 μM). The solid lines are the best fits of the data by the general solution for burst kinetics (eq 2) with the rate constants given in Table 1.

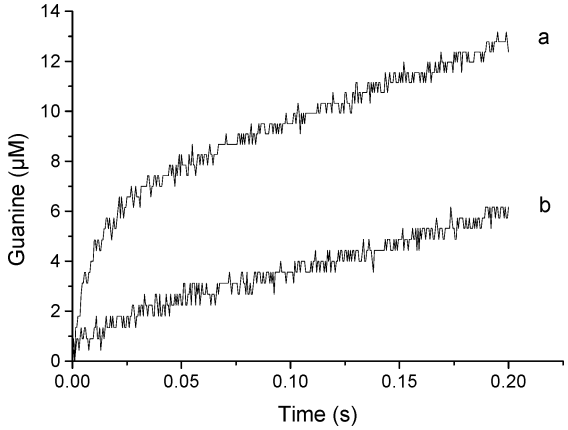

FIGURE 2: Kinetics of guanosine hydrolysis by free and ribose bound NH. Trace a, 12 μM NH mixed with 50 μM guanosine and trace b, 12 μM NH mixed with 50 μM guanosine, both premixed with 5 mM ribose.

The occurrence of a pre-steady-state product burst at an excess of substrate implies that all the steps before the rate-limiting step in the steady-state phase are fast (*13*) and that the rate-limiting step follows the hydrolysis of the *N*-glycosidic bond. These results suggest that ribose release is rate limiting. To address this point, the hydrolase was preincubated with an excess of ribose (5 mM) and mixed with the substrate guanosine. It was found that binding of the product ribose in the active site, prior to binding of the substrate guanosine, significantly attenuates the magnitude of the burst (Figure 2). We inferred that this attenuation is due to a significant amount of enzyme that has bound ribose during preincubation. For this fraction, the whole process including the first turnover occurs at a rate corresponding to the rate-limiting step (i.e., the ribose release). All data can conveniently be explained according to reaction scheme shown in Table 1, where $k_3 < k_2$. The experimental traces have been fitted to the general equation (eq 2) for this mechanism (*12*).

For the different enzyme concentrations used (Figure 1), the burst-rate of guanine production (k_2) consistently fitted around 76 s^{-1}. In all measurements, a slow release of the ribose moiety (k_3) at 3.4 s^{-1} followed this burst (Table 1). The experiments were repeated for adenosine and inosine.

Table 1: Burst Kinetics of Guanosine Hydrolysis[a]

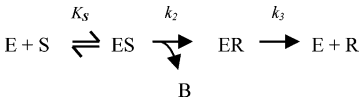

substrate	k_2 (s^{-1})	k_3 (s^{-1})
guanosine	76 ± 2.7	3.4 ± 0.4
inosine	230 ± 20	3.6 ± 0.4
adenosine	105 ± 2	3.0 ± 0.4

[a] The association of the substrate (K_S) is very fast as compared to the subsequent steps. Data ± standard deviation were a result from averaging the best fits to eq 2 of three individual stopped-flow absorption experiments using variable enzyme concentrations.

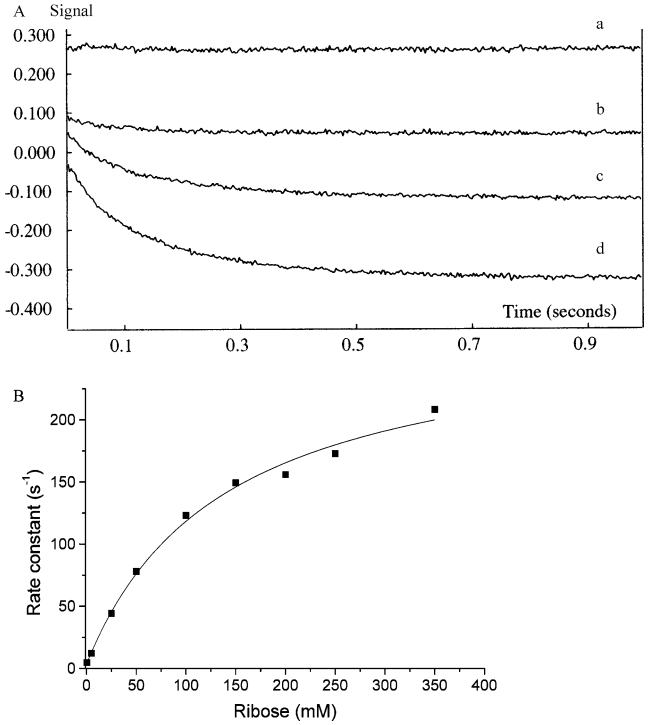

FIGURE 3: Kinetics of ribose binding. (A) Fluorescence transients obtained upon mixing constant amounts of NH (3.8 μM) with various amounts of ribose. Trace a, 0 mM ribose; trace b, 1 mM ribose; trace c, 5 mM ribose; and trace d, 10 mM ribose. (B) The apparent rate constant (k_{obs}) for ribose binding for the complete ribose concentration range (0.25−350 mM) used in the stopped-flow fluorescence experiment. The solid line corresponds to the best-fit curve according to the scheme and rate constants of Table 2.

The conversion of these substrates by the nucleoside hydrolase also follows burst kinetics. All experimental results are summarized in Table 1.

Two-Step Ribose Binding. Considering that ribose release is slow, we studied the kinetics of the binding of ribose to the *T. vivax* IAG-NH using stopped-flow fluorescence. For this purpose, different amounts of ribose (0.25−350 mM) were mixed with a fixed amount of enzyme (4 μM). A number of representative fluorescence transients are shown in Figure 3A. All fluorescence transients could be adequately fitted to a single exponential. Analysis of the observed rates (k_{obs}) over the complete concentration range shows a hyperbolic dependence on the ribose concentration (see Figure 3B). The hyperbolic increase of k_{obs} with increasing ribose concentration is in agreement with a reaction scheme comprising a very fast bimolecular step followed by a slow

Table 2: Kinetics of Ribose Binding[a]

$$E + R \underset{}{\overset{K_S}{\rightleftharpoons}} ER \underset{k_{-2}}{\overset{k_2}{\rightleftharpoons}} ER'$$

K_S (mM)	k_2 (s^{-1})	k_{-2} (s^{-1})	K_{SO} (mM)[b]
140 ± 20	274 ± 13	4.3 ± 2.4	2 ± 1

[a] Data given represent the best fits of the stopped-flow fluorescence traces to eq 4. [b] K_{so}, the global dissociation constant, was derived from eq 5.

unimolecular step (*14*) (Table 2), where the relaxation times of these two steps are on different time scales. The concentration dependence of k_{obs} is appropriately fitted to a model accounting for a two-step binding process including a fast association/dissociation process (K_S), followed by a slow conformational change (k_2 and k_{-2}) (eq 4). The best-fit results for the rate constants are summarized in Table 2.

Two-Step Substrate Binding. Considering that the ribose binding process involves a slow conformational change, we also analyzed the process of substrate binding by itself using stopped-flow fluorescence experiments following two strategies. First, we analyzed the binding curves of guanosine to the Asp10Ala mutant. This sluggish mutant of the *T. vivax* IAG-NH is missing the essential catalytic proton acceptor Asp10 and needs 28 min to convert 1 equivalent of substrate into product (*10*). The fluorescence transients observed after rapid mixing of different amounts of guanosine (25 μM to 1.5 mM) with a fixed amount of the Asp10Ala mutant (4 μM) were indicative for two relaxation processes and had to be fitted by a sum of two exponentials. Hence, two relaxations are observed in the same time scale, implying that the binding process consists of at least two elementary steps. To estimate the microscopic rate constants of the process, two different fitting methods were performed. In a first procedure, the obtained relaxation times were fitted to the general solution (eq 3) for a two-step reversible binding process (*14*). All microscopic rate constants were derived from the linear regressions on the sum and the product of this general solution of the observed relaxation rates (*14*) (fitting procedure 1 in Table 3). In a second procedure, all traces were simultaneously fitted to a two-step reversible binding model with the program Pro-KII (fitting procedure 2 in Table 3).

We also followed the binding of the nonhydrolyzable substrate analogue 3-deaza adenosine to the wild-type enzyme by stopped-flow fluorescence. Various amounts of this inhibitor (0.15−90 μM) were mixed with the wild-type enzyme (4 μM). Because of the high affinity of 3-deaza adenosine, it was impossible to work under pseudo-first-order conditions. Therefore, the relaxation traces were simultaneously fitted to the two-step reversible binding model with the program Pro-KII (fitting procedure 2 in Table 3).

Multiple Turnover Experiments. Aiming to study the interconversion rates of the different transient intermediates, multiple turnover experiments were performed using stopped-flow fluorescence. For this purpose, we mixed various amounts of the genuine substrate guanosine (2−60 μM) with the wild-type enzyme (2.5 μM). A number of prototypical fluorescence transients are shown in Figure 4.

The microscopic constants of the proposed reaction scheme were obtained with the program Pro-KII. The software allowed us to simultaneously fit 22 fluorescence traces to the scheme shown in Table 4, following an iterative process. Initially, a global model (including two-step substrate binding and two-step product release) was used to derive all interconversion rates of the different transient intermediates at once. Such a model proved to contain too many variables to provide appropriate fits to the experimental results. By reducing the two-step product release to a single bimolecular process, a first reduction of the number of parameters was achieved (Table 4). The burst kinetics and ribose binding experiments with the wild-type NH provide a very good estimate of the rate constants of base and ribose release (k_3, k_4, and k_{-4} in Table 4) in the overall reaction mechanism. In contrast, from the previous substrate binding measurements, we can only draw mechanistic conclusions without quantitative interpretation of the absolute values. Finally, the rate constants of substrate binding in the overall reaction mechanism could be obtained by introducing the rate constants derived from the burst kinetics and ribose binding experiments in the fitting procedure (Table 4).

Steady-State Parameters. To validate the calculated microscopic rate constants based on the proposed reaction mechanism, we determined the steady-state kinetic parameters for guanosine under the same experimental conditions. Therefore, various amounts of the substrate (2−60 μM) were mixed with the wild-type enzyme (0.35 μM) to follow the steady-state formation of guanine using stopped-flow absorption. The k_{cat} is expressed per homodimer to account for the observed half-of-the-sites reactivity. The resulting steady-state parameters are given in Table 4.

DISCUSSION

All parasitic protozoa lack the ability to synthesize purine nucleotides de novo (*15*−*17*). Instead, they use salvage enzymes to obtain purine bases and nucleosides from their hosts and convert them to the corresponding nucleotides. The nucleoside hydrolases play a key role in these purine salvage pathways. Considering their function as scavengers, the catalytic performance of most parasitic hydrolases seems rather poor. Interestingly, most hydrolases convert a number of different substrates with comparable steady-state kinetic parameters (e.g., inosine, adenosine, and guanosine for the IAG-specific NH from *T. vivax*). Also, mutations in the active site of the IAG-specific hydrolase of *T. vivax* exert little effect on k_{cat} and K_M. All these data suggest that these macroscopic constants are combinations of various rate and equilibrium constants for which the result is little sensitive to the chemical properties of the base or the susceptibility of the scissile bond. Here, we describe the kinetics of guanosine conversion by the nucleoside hydrolase of *T. vivax* as studied by a combination of steady-state and pre-steady-state analysis by means of stopped-flow absorption and stopped-flow fluorescence experiments.

Product Release as Rate-Limiting Step in the Hydrolysis of Nucleosides. The pre-steady-state enzymatic formation of guanine from guanosine, measured by stopped-flow absorbance, shows burst kinetics. Preincubation of the enzyme with saturating amounts of ribose attenuates mostly the burst, indicating that the slow release of ribose follows a fast catalytic step that includes the release of the base. Similarly, the steady-state hydrolysis of adenosine and inosine is

Table 3: Kinetics of Substrate Binding[a]

$$E + S \underset{k_{-1}}{\overset{k_1}{\rightleftharpoons}} ES \underset{k_{-2}}{\overset{k_2}{\rightleftharpoons}} ES'$$

		k_1 (μM^{-1} s^{-1})	k_{-1} (s^{-1})	k_2 (s^{-1})	k_{-2} (s^{-1})	K_{SO}[d] (μM)
guanosine[b]	fitting procedure 1	0.25	52	11	10	101
guanosine[b]	fitting procedure 2	0.26 ± 0.02	37 ± 4	8.0 ± 1.3	9.2 ± 0.6	75 ± 30
3-deaza adenosine[c]	fitting procedure 2	5.1± 0.5	47 ± 1	22.2 ± 0.9	26.9 ± 0.2	5.0 ± 0.5

[a] Data given represent the best fit of the stopped-flow fluorescence traces, following two alternative fitting strategies (see text). [b] Analysis of the binding kinetics of genuine substrate guanosine to the Asp10Ala mutant of *T. vivax* NH. [c] Analysis of the binding kinetics of the nonhydrolyzable substrate analogue 3-deaza adenosine to the wild-type *T. vivax* NH. [d] K_{SO}, the overall dissociation constant, was derived from eq 5.

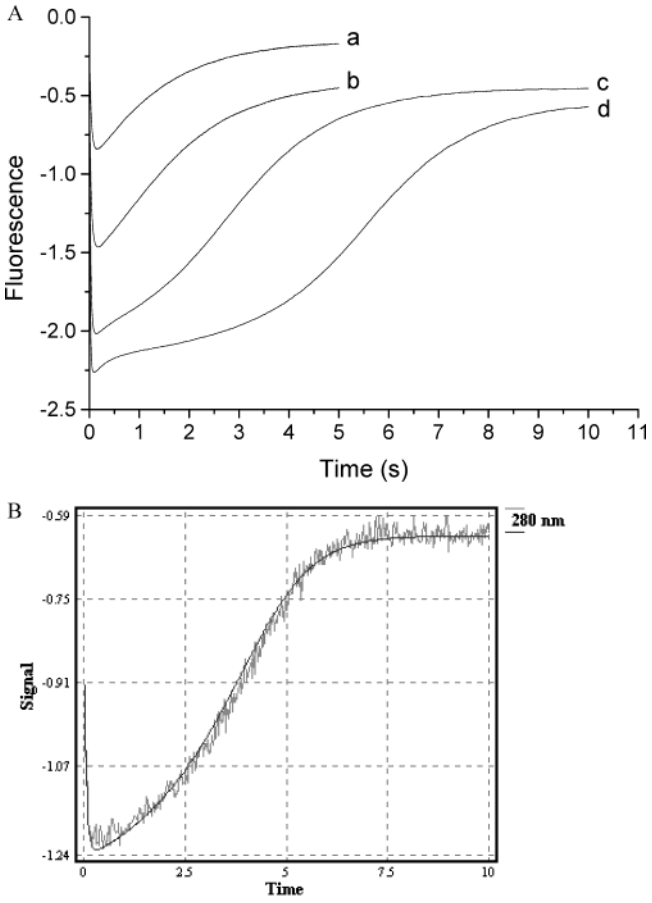

FIGURE 4: Stopped-flow fluorescence analysis of guanosine conversion by *T. vivax* NH. (A) Experimental fluorescence transients obtained after mixing fixed amounts of NH (2.5 μM) with various concentrations of the substrate guanosine. Trace a, 5 μM guanosine; trace b, 10 μM guanosine; trace c, 25 μM guanosine; and trace d, 60 μM guanosine. (B) The best-fit curve (solid line) on one experimental fluorescence trace, obtained after mixing 10 μM guanosine and 2.5 μM NH, according to the scheme and rate constants of Table 4.

preceded by a burst of the corresponding bases. All experimental data could conveniently be fitted according to a model where substrate binding is much faster as compared to a subsequent fast chemical step and a slow release of the ribose (Table 1). The chemical conversion rate (k_2) is much faster than the steady-state turnover rate, which is limited by ribose release. The rate of ribose release is slower and independent of the kind of substrate used. This explains why the purines are hydrolyzed with comparable catalytic rates (k_{cat}) under steady-state conditions.

Half-of-the-Sites Reactivity. The burst of product formation during the first turnover allows us to establish the absolute concentration of active sites (*12*). Indeed, the catalytic step for guanosine hydrolysis (k_2) is fast enough, as compared to the release of ribose (k_3). As a result, the magnitude of the burst is equal to the concentration of active sites. During our active site titration of the enzyme with guanosine, we found that the concentration of active sites that contribute to the first turnover is only half the amount of monomeric enzyme used. Considering that the *T. vivax* IAG-NH is a dimer, consisting of two identical monomers, it appears that the enzyme exhibits half-of-the-sites reactivity. However, crystals of the *T. vivax* NH in complex with substrate did contain two bound substrates per dimer. This might be explained by the very high substrate concentration used in the crystal setups. For the related trimeric nucleoside phosphorylases of calf spleen acting in the same purine salvage pathway, a third-of-the-sites reactivity has been described (*18*). The molecular mechanism for this extreme form of negative cooperativity is not known for the hydrolase, nor for the phosphorylases. A number of mechanisms can be envisioned (*19*). First, polypeptides can dimerize in an asymmetric way so that the conformations of the two active sites are not identical. The crystal structure of the free *T. vivax* dimer does not sustain this formal possibility. In the dimer, the active sites of the hydrolase are at a distance of ≈28 Å, which is to far away for one substrate molecule to block the binding of another one by steric or electrostatic exclusion. Alternatively, binding of one substrate can induce conformational changes in the other active site so that the second site is turned off. Considering its position in the dimer, a flexible loop that is located in the vicinity of the active site (*10*) (Figure 5) might also account for the half-of-the-site reactivity of the *T. vivax* enzyme. Indeed, in case this loop should close above the active site upon binding of the substrate, it might sterically hinder access to the second active site. So far, we have no experimental evidence to sustain particular mechanisms.

Ribose Release Involves a Rate-Limiting Conformational Change. Stopped-flow fluorescence experiments were set out to examine the binding of the product ribose in the pre-steady-state. The apparent association rate (k_{obs}) was found to display a hyperbolic dependence on the ribose concentration. This kinetic feature is consistent with a two-step mechanism (Table 2), in which a slow unimolecular isomerization process follows a fast bimolecular association. This isomerization results in a tightly bound enzyme−ribose complex (ER′ in Table 2) (*20*). It is striking that the rate-

Table 4: Kinetic Constants of *T. vivax* NH Using Guanosine as a Substrate[a]

$$E + S \underset{k_{-1}}{\overset{k_1}{\rightleftharpoons}} ES \underset{k_{-2}}{\overset{k_2}{\rightleftharpoons}} ES' \overset{k_3}{\rightarrow} B \quad ER \underset{k_{-4}}{\overset{k_4}{\rightleftharpoons}} E + R$$

k_1 ($\mu M^{-1} s^{-1}$)	k_{-1} (s^{-1})	k_2 (s^{-1})	k_{-2} (s^{-1})	k_3 (s^{-1})	k_4 (s^{-1})	k_{-4} ($\mu M^{-1} s^{-1}$)	k_{cat}^{calc} (s^{-1})	k_{cat}^{obs} (s^{-1})	K_M^{calc} (μM)	K_M^{obs} (μM)
1.8±0.2	80 ± 20	150 ± 27	1 ±12	76 ± 2.7	3.77 ± 0.4	0.002 ± 0.0005	3.5 ± 0.5	3.52 ± 0.05	5.3 ± 0.9	5.6 ± 0.8

[a] Data shown represent the best-fit parameters of the fluorescence stopped-flow traces. The steady-state kinetic parameters k_{cat}^{calc} and K_M^{calc} were calculated from the microscopic rate constants according to eq 6. The steady-state kinetic parameters k_{cat}^{obs} and K_M^{obs} were determined in the steady-state assays.

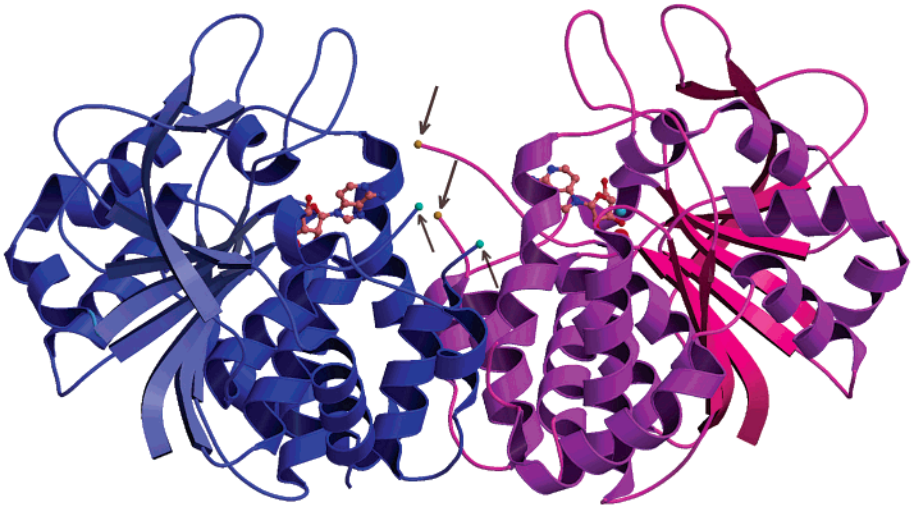

FIGURE 5: Location of the flexible loop in the structure of the *T. vivax* IAG-NH dimer in complex with 3-deaza adenosine (PDB entry 1HP0). The 3-deaza adenosine molecules located in each active site of the dimer are shown as ball-and-stick models, and the calcium ions are depicted as red spheres. Because of the flexibility of the loop, amino acids 248−255 and 248−252 (indicated by arrows) were excluded from the model in monomer A (shown in blue) and monomer B (shown in violet), respectively. This figure was made with MOLSCRIPT (*24*).

limiting step of the enzyme catalyzed hydrolysis of the purine nucleosides (k_3 in Table 1) and the slow unimolecular isomerization step during ribose dissociation (k_{-2} in Table 2), necessary to convert the tightly bound enzyme−ribose complex into the fast dissociating loosely bound complex, take place with comparable rates. All data indicate that the tightly bound enzyme−ribose complex accumulates during the enzymatic hydrolysis of the common purine nucleosides because a slow isomerization between a tight and a loose enzyme−ribose complex is the rate-limiting step on the reaction coordinate.

Substrate Binding Involves a Conformational Change. Because slow unimolecular isomerization processes are important in product release, we also searched for the accumulation of particular substrate-bound intermediates by stopped-flow fluorescence. In general, it is difficult to investigate the binding process of substrates because they are enzymatically converted to products. To circumvent this problem, we investigated the binding of the nonhydrolyzable substrate analogue 3-deaza adenosine to wild-type enzyme and the binding of the genuine substrate guanosine to the sluggish Asp10Ala mutant, respectively. In both cases, the binding was found to follow a two-step association mechanism. Similar to ribose binding, a loosely bound ES complex is formed rapidly. This loose complex is then converted slowly into a tighter ES′ complex in a unimolecular event (Table 3). The nature of the isomerization is unclear. There is no crystallographic evidence for large conformational changes in the protein structure upon binding of 3-deaza adenosine to wild-type enzyme (*5*). A little shift in the conformation of Trp83 upon inhibitor binding induced Trp83 to align perfectly parallel with the nucleic base, causing favorable face-to-face aromatic stacking interactions. However, ribose binding proceeds through the same unimolecular isomerization, indicating that interactions with the purine are not fundamental for the conformational changes. The crystal structure of the Asp10Ala mutant in complex with inosine showed a C'_4 endo envelope for the ribose moiety of the substrate (*10*). The same conformation was also observed for the transition state analogue *p*-aminophenyliminoribitol (pAPIR) bound to the IU-NH of *C. fasciculata* (*21*). This conformation differs from the most stable conformations in solution (C'_2 endo or C'_3 endo) (*22*). The conformational change from C'_2 endo or C'_3 endo to C'_4 endo could be a slow but critical event to increase the chemical reactivity of the scissile bond and may be at the origin of the slow unimolecular isomerization observed in the binding experiments.

From Pre-Steady State to Steady State. All pre-steady-state experiments support a multistep reaction mechanism including fast binding of the substrate, followed by the unimolecular formation of a tight enzyme−substrate complex that is converted enzymatically into a tight ribose bound intermediate. In a slow rate-limiting step, this tight enzyme−ribose complex is converted into a loose complex from which the sugar dissociates. To consolidate this model, multiple

turnover stopped-flow fluorescence experiments were performed (Figure 5). A minimal model was used to derive all interconversion rates (Table 4). This mechanism includes a two-step association of the substrate, a fast base release, and slow ribose release. Using the determinant method described by King and Altman (*23*), we derived the expressions for the steady-state parameters (eq 6) according to the reduced four-step reaction mechanism (Table 4)

$$k_{cat} = k_4k_2k_3/[k_4(k_{-2} + k_2) + k_3(k_4 + k_2)] \text{ and}$$
$$K_M = k_4(k_{-1}k_2 + k_{-1}k_3 + k_2k_3)/[k_1(k_4k_{-2} + k_4k_3 + k_4k_2 + k_2k_3)] \quad (6)$$

This allowed us to confirm that the reduced four-step reaction mechanism and the corresponding microscopic rate constants are in agreement with the steady-state kinetic parameters, derived for guanosine.

We conclude that the nucleoside hydrolase from *T. vivax* follows a complex multistep reaction mechanism where a nonchemical step is rate limiting. The slow common step is an isomerization between a tight and a loose enzyme−ribose complex, causing an accumulation of the tightly bound enzyme−ribose complex during the enzymatic hydrolysis of the common purine nucleosides. Whether such a complex multistep mechanism also applies for other members of the nucleoside hydrolase family remains to be explored.

ACKNOWLEDGMENT

The authors thank Dr. D. Maes for the excellent mathematical assistance.

REFERENCES

1. Bzowska, A., Kulikowska, E., and Shugar, D. (2000) Purine nucleoside phosphorylase: properties, functions, and clinical aspects, *Pharmacol. Ther. 88*, 349−425.
2. Seegmiller, J. E., Rosenbloom, F. M., and Kelley, W. N. (1967) Enzyme defect associated with a sex-linked human neurological disorder and excessive purine synthesis, *Science 155*, 1682−1684.
3. Aronov, A. M., Munagala, N. R., de Montellano, P. R. O., Kuntz, I. D., and Wang, C. C. (2000) Rational Design of Selective Submicromolar Inhibitors of *Trichichomonas foetus* Hypoxanthine−Guanine−Xanthine Phosphoribosyltransferase, *Biochemistry 39*, 4684−4691.
4. Parkin, D. W., Horenstein, B. A., Abdulah, D. R., Estupiñán, B., and Schramm, V. L. (1991) Nucleoside Hydrolase from *Crithidia fasciculata*. Metabolic role, purification, specificity, and kinetic mechanism, *J. Biol. Chem. 266*, 20658−20665.
5. Versées, W., Decanniere, K., Pellé, R., Depoorter, J., Brosens, E., Parkin, D. W., and Steyaert, J. (2001) Structure and function of a novel purine specific nucleoside hydrolase from *Trypanosoma vivax*, *J. Mol. Biol. 307*, 1363−1379.
6. Parkin, D. W. (1996) Purine-specific nucleoside *N*-ribohydrolase from *Trypanosoma brucei* brucei. Purification, specificity, and kinetic mechanism, *J. Biol. Chem. 271*, 21713−21719.
7. Estupiñán, B., and Schramm, V. L. (1994) Guanosine-inosine-preferring nucleoside *N*-glycohydrolase from *Crithidia fasciculata*, *J. Biol. Chem. 269*, 23068−23073.
8. Horenstein, B. A., Parkin, D. W., Estupiñán, B., and Schramm, V. L. (1991) Transition-State Analysis of Nucleoside Hydrolase from *Crithidia fasciculata*, *Biochemistry 30*, 10788−10795.
9. Horenstein, B. A., and Schramm, V. L. (1993) Correlation of the electrostatic potential surface of an enzymatic transition state with novel transition-state inhibitors, *Biochemistry 32*, 9917−9925.
10. Versées, W., Decanniere, K., Van Holsbeke, E., Devroede, N., and Steyaert, J. (2002) Enzyme−substrate interactions in the purine-specific nucleoside hydrolase from *Trypanosoma vivax*, *J. Biol. Chem. 277*, 15938−15946.
11. Pace, C. N., Vajdos, F., Fee, L., Grimsley, G., and Gray, T. (1995) How to measure and predict the molar absorption coefficient of protein, *Protein Sci. 4*, 2411−2423.
12. Cornish-Bowden, A. (1995) *Fundamentals of enzyme kinetics*, Portland Press Ltd., New York.
13. Johnson, K. A (1992) *Enzymes 20*, 1−61.
14. Fersht, A. R. (1985) *Enzyme Structure and Mechanism*, W. H. Freeman and Company, New York.
15. Ogbunude, P. O. J., Ikediobi, C. O., and Ukoha, A. I. (1985) Adenosine cycle in African trypanosomes, *Ann. Trop. Med. Parasitol. 79*, 7−11.
16. Hammond, D. J., and Gutteridge, W. E. (1984) Purine and pyrimidine metabolism in the trypanosomatidae, *Mol. Biochem. Parasitol. 13*, 243−261.
17. Berens, R. L., Krug, E. D., and Marr, J. J. (1995) in *Biochemistry and Molecular Biology of Parasites* (Marr, J. J., and Müller, M.) pp 89−117, Academic Press, New York.
18. Kline, P. C., and Schramm, V. L. (1992) Purine nucleoside phosphorylase. Inosine hydrolysis, tight binding of the hypoxanthine intermediate, and third-the-sites reactivity, *Biochemistry 31*, 5964−5973.
19. Levitzki, A., Stallcup, W. B., and Koshland, D. E., Jr. (1971) Half-of-the-sites reactivity and the conformational states of cytidine triphosphate synthetase, *Biochemistry 10*, 3371−3378.
20. Hiromi, K. (1979) *Kinetics of Fast Enzyme Reactions*, John Wiley & Sons, New York.
21. Degano, M., Almo, S. C., Sacchetini, J. C., and Schramm, V. L. (1998) Trypanosomal Nucleoside Hydrolase. A Novel Mechanism from the Structure with a Transition-State Inhibitor, *Biochemistry 37*, 6277−6285.
22. Gelbin, A., Schneider, B., Clowney, L., Hsieh, S.-U., Olson, W. K., and Berman, H. M. (1996) Geometric Parameters in Nucleic Acids: Sugar and Phosphate Constituents, *J. Am. Chem. Soc. 118*, 519−529.
23. King, E. L., and Altman, C. (1956) *J. Phys. Chem. 60*, 1375−1378.
24. Kraulis, P. J. (1991) MOLSCRIPT: a program to produce both detailed and schematic plots of protein structures, *J. Appl. Crystallogr. 24*, 946−950.

BI0347914